Available online at www.sciencedirect.com
ScienceDirect
Journal of the European Ceramic Society 31 (2011) 855–862
www.elsevier.com/locate/jeurceramsoc

Ultra-high temperature ablation behavior of Ti_2AlC ceramics under an oxyacetylene flame

G.M. Song [a,*], S.B. Li [a], C.X. Zhao [a], W.G. Sloof [a], S. van der Zwaag [b], Y.T. Pei [c], J.Th.M. De Hosson [c]

[a] Department of Materials Science and Engineering, Delft University of Technology, Delft, Mekelweg 2, 2628 CD Delft, The Netherlands
[b] Novel Aerospace Materials Group, Faculty of Aerospace Engineering, Delft University of Technology, Kluyverweg 1, 2629 HS Delft, The Netherlands
[c] Department of Applied Physics, The Netherlands Materials Innovation Institute M2i and Zernike Institute for Advanced Materials, University of Groningen, Nijenborgh 4, 9747 AG Groningen, The Netherlands

Received 2 September 2010; received in revised form 16 November 2010; accepted 28 November 2010
Available online 17 December 2010

Abstract

The linear and mass ablation rates of Ti_2AlC ceramics under an oxyacetylene flame at a temperature up to 3000 °C were examined by measuring the dimensions and weight change of the ablated samples. The linear ablation rate was decreased from 0.14 μm s^{-1} for the first 30 s of the ablation to 0.08 μm s^{-1} after 180 s. Ti_2AlC ceramics gained small amounts of weight upon ablation, which is attributed to the formation of oxidation products on the ablated surface. The ablation surface exhibits a two-layer structure: an oxide outer layer, consisting mainly of α-Al_2O_3 and TiO_2 and some Al_2TiO_5, and a porous sub-surface layer containing $Ti_2Al_{1-x}C$ and TiC_xO_y. With increasing ablation time, the content of TiO_2 and Al_2TiO_5 in the outer layer increased, and more pores developed in the sub-surface layer. The thermal oxidation of Ti_2AlC under the flame and scouring of the viscous oxidation products by high-speed flow of gas torch are the main ablation mechanisms.

Keywords: Ti_2AlC; Ablation; Oxyacetylene flame; Oxidation

1. Introduction

Ti_2AlC is a typical example of atomically layered ternary carbides belonging to the so-called MAX phase family.[1] Recently, it has attracted scientific and commercial attention due to its excellent isothermal and thermal cycling oxidation resistance in combination with its high electrical conductivity, resistance against thermal shock and strengths at high temperatures.[2–6] The low oxidation rate is caused by the formation of a continuous protective α-Al_2O_3 layer on the Ti_2AlC substrate, and the superior spallation resistance of the α-Al_2O_3 layer is attributed to the well-matched thermal expansion coefficients between α-Al_2O_3 layer and Ti_2AlC substrate.[5,6] Based on this, it is likely that Ti_2AlC may withstand ultra-high temperatures for relatively short times since Ti_2AlC will decompose into sub-stoichiometry Ti_2Al_xC or even twinned $TiC_{0.5}$ superstructure and Al rather than becoming a liquid phase itself as long as the temperature does not exceed the melting point (~3250 °C) of TiC_x ($x = 0.5$–1).[7–9] Therefore, Ti_2AlC is probably a promising candidate for thermal structural components exposed to ultra-high temperature ablative environments such as nose caps of missiles, rudders and nozzles of rocket engines, gas burners and heat shields in nuclear power stations and other high temperature components, where ablation is a critical material behavior aspect. Hence it is relevant to investigate the ablation properties of Ti_2AlC in ultra-high temperature environments, which have not been scrutinized before. In this paper, the ultra-high temperature ablation behavior of Ti_2AlC ceramics using a conventional oxyacetylene flame is presented.

2. Experimental

Bulk Ti_2AlC ceramic samples were prepared via an in situ solid–liquid reaction between Ti, Al and graphite powders, heated to a high temperature. Ti, Al and graphite powders with the desired atomic ratio of 2:1.1:1 were mixed by ball-milling

* Corresponding author. Tel.: +31 15 2782480; fax: +31 15 2786730.
E-mail address: g.song@tudelft.nl (G.M. Song).

0955-2219/$ – see front matter.
doi:10.1016/j.jeurceramsoc.2010.11.035

for 20 h in an ethanol solution. The slurry was dried at 60 °C and cold-pressed into blocks with 8 MPa in a graphite die, and then hot-pressed with 30 MPa at 1450 °C for 5 h in flowing argon gas. Disk shaped samples with a size of 30 mm in diameter and 10 mm in thickness were cut from the sintered bulk Ti_2AlC by using electrical discharge wire machining for ablation tests. The planar surfaces of the disks were grinded using SiC emery papers with 400 down to 1200 grit, followed by polishing with 1 μm diamond paste. The ablation tests were implemented according to the standard GJB 323A-96 with an oxyacetylene flame.[10,11] The pressure and the flow rate of acetylene were respectively, 0.095 MPa and 1.116 $m^3\ h^{-1}$, and the pressure and the flow rate of oxygen were respectively, 0.4 MPa and 1.512 $m^3\ h^{-1}$. The distance between the flame gun mouth and ablation surface of the disk was fixed at 10 mm. The centres of the flame and the torch were aligned horizontally. Under such conditions the material to be tested would be locally exposed to a flame temperature up to 3000 °C[10–12] leading to hot gas flow induced material removal.

The resulting linear ablation rate, R_d, and the mass ablation rate, R_m, are defined as:

$$R_d = \frac{(d_t - d_0)}{t} \quad (1)$$

$$R_m = \frac{(m_t - m_0)}{t} \quad (2)$$

where d_0 and d_t represent the thicknesses of the disk measured at the surface centre position of a sample before and after the ablation time t, respectively. m_0 and m_t are the weights of the sample before and after ablation. The dynamical ablation process was recorded by a high-speed camcorder with a speed of 1000 frames per second (Phantom V5, equipped with a 70–300 mm Nikon optical lens and an ultraviolet glass filter) and a digital camera (Nikon D90) with a much slower framing rate.

The morphology and chemical composition of the ablated surfaces as well as cross-sections of the disk samples were examined with a scanning electronic microscope (SEM, JSM 6500F) equipped with an energy dispersive spectrometer (EDS, Noran Pioneer 30 mm^2 Si(Li) detector) for chemical composition analysis. The cross sections of the ablated samples were prepared with a cross section ion polisher (JEOL SM-09010) which effectively minimizes polishing induced artifacts.[13,14] The ablation products at the ablated surface centre were analyzed with an X-ray diffractometer (XRD, Bruker AXS D5005 XRD) equipped with a Vantec position sensitive detector and graphite monochromator. The pattern data collection was carried out using monochromatic Cu Kα radiation in the 2θ region between 20° and 80° with a step size of 0.03° in 2θ and step time of 2 s. The sample was placed on a Si {5 1 0} substrate and rotated during measurement. The X-ray beam with a size of 8 mm in height and 1 mm in width was used to scan the ablated surfaces. The lamellar Ti_2AlC grain in the sintered Ti_2AlC has a width of about 5–20 μm and a length from about 20 to 100 μm, as shown in Fig. 1. The porosity of the material was measured as 1.1 vol% by analyzing several back electron scattering images taken from polished surfaces with image analysis software ImageJ.[15]

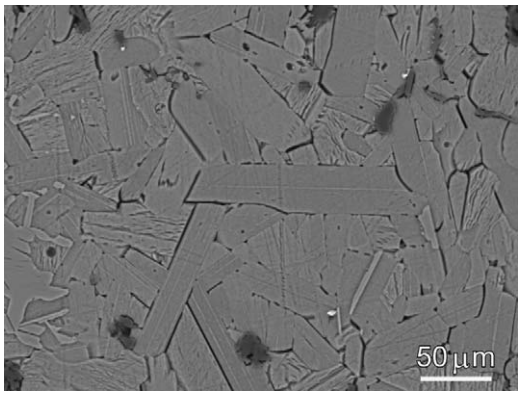

Fig. 1. Micrograph of Ti_2AlC ceramics etched in a 1:1:1 by volume $HF:HNO_3:H_2O$ solution, showing Ti_2AlC lamellar grains and small amount of Al_2O_3 particles (dark phase).

3. Results and discussion

3.1. Ablation properties

The linear and mass ablation rates as a function of the ablation time for the Ti_2AlC samples are plotted in Fig. 2. The linear ablation rate was 0.14 μm s^{-1} during the initial 30 s, and decreased to 0.085 μm s^{-1} when the ablation time exceeded 180 s. Such a decrease in the linear ablation rate with ablation time is generally attributed to the formation of an ablation layer on the base material. Similar decreases have also been observed in other ultra-high temperature materials, such as tungsten and ZrC and TiC reinforced tungsten composites.[16,17] It is noteworthy that the mass ablation rate of Ti_2AlC measured in this study was −270 μg s^{-1} at the onset of ablation (30 s) and −180 μg s^{-1} for ablating 180 s, which means that the present ablation resulted in a mass gain rather than a mass loss (Fig. 1). This mass gain behavior is contrary to ablation behavior of some ultra-high temperature materials, such as carbon/carbon,[18] Cu-infiltrated tungsten and tungsten composites,[16,17] in which mass loss caused a positive mass ablation rates (i.e. $R_m > 0$). The ablation properties of the Ti_2AlC studied here are listed in Table 1 together with some modern ultra-high temperature materials tested with oxyacetylene flame according to the same standard GJB 323A-96.[10] Compared to these ultra-high temper-

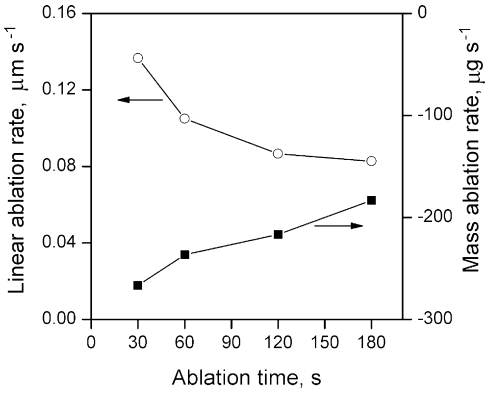

Fig. 2. Linear and mass ablation rates of Ti_2AlC ceramics.

Table 1
Linear ablation rates of several high temperature materials (ablation time: 60 s).

Materials	Linear ablation rate ($\mu m\,s^{-1}$)	Mass ablation rate ($\mu g\,s^{-1}$)	Ref.
Ti_2AlC	0.11	−240	Present
Pure W	13.6	47	[14]
Cu-infiltrated W	11.7	85	[13]
40 vol%TiC/W composite	4.2	19	[14]
40 vol%ZrC/W composite	2.4	10	[14]
C/C (CVI) composite	3.0	2700	[15]
4.14 wt.%ZrC-doped C/C composite	0.51	620	[15]

ature materials, Ti_2AlC possesses an extreme low linear ablation rate, viz. 0.11 $\mu m\,s^{-1}$ for 60 s ablation, which is close to zero. Such a low ablation rate may ensure a stable shape profile if Ti_2AlC is to be used in ultra-high temperature ablative environments.

3.2. Ablated microstructure

The pictures recorded of the ablation process of a Ti_2AlC disk sample under a glaring oxyacetylene flame are shown in Fig. 3. With an ultraviolet glass filter, the spreading of the temperature field of the disk upon ablation was revealed with the evolution of high temperature zone propagating from the surface centre to the periphery, which implies that the centre zone experienced severer ablation than the peripheral area. The ablated surfaces after ablation for 30 s and 180 s are presented in Fig. 4. A very shallow concave impression with a diameter of about 2 mm formed at the centre of the surface area (Fig. 4(a) and (c)), which was caused by the oxidation and the scouring of the viscous oxidation products under the high-speed gas flow. When the ablation time increased from 30 s to 180 s, the color of the ablated surface changed from grey to light yellow, but the white color of the centre zone kept unchanged; see Fig. 4(a) and (c). Fig. 4(b) is a high magnification image of the ablation centre zone of the sample ablated for 30 s (Fig. 4(a)). (For interpretation of the references to color in text, the reader is referred to the web version of the article.) The microstructure analysis with SEM/EDS and XRD on the centre zone reveals that there are

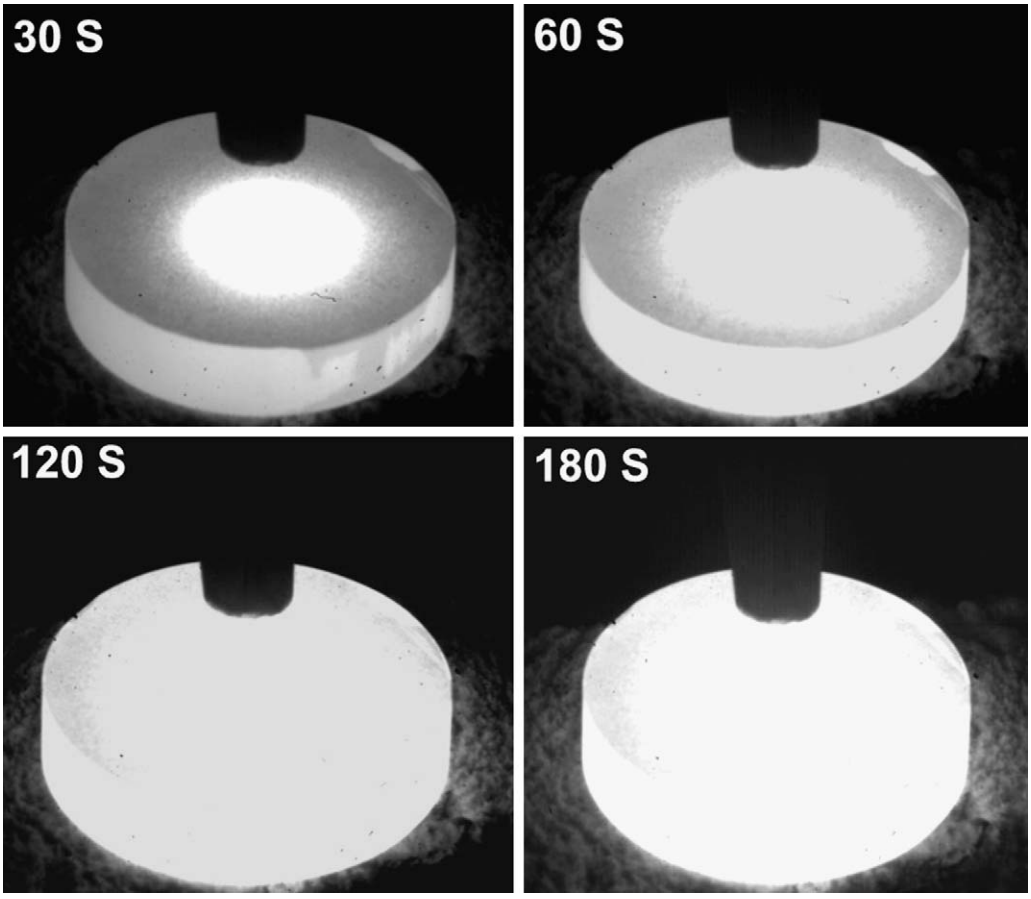

Fig. 3. Ti_2AlC disk sample exposed to oxyacetylene flame with a temperature up to 3000 °C at various exposure times.

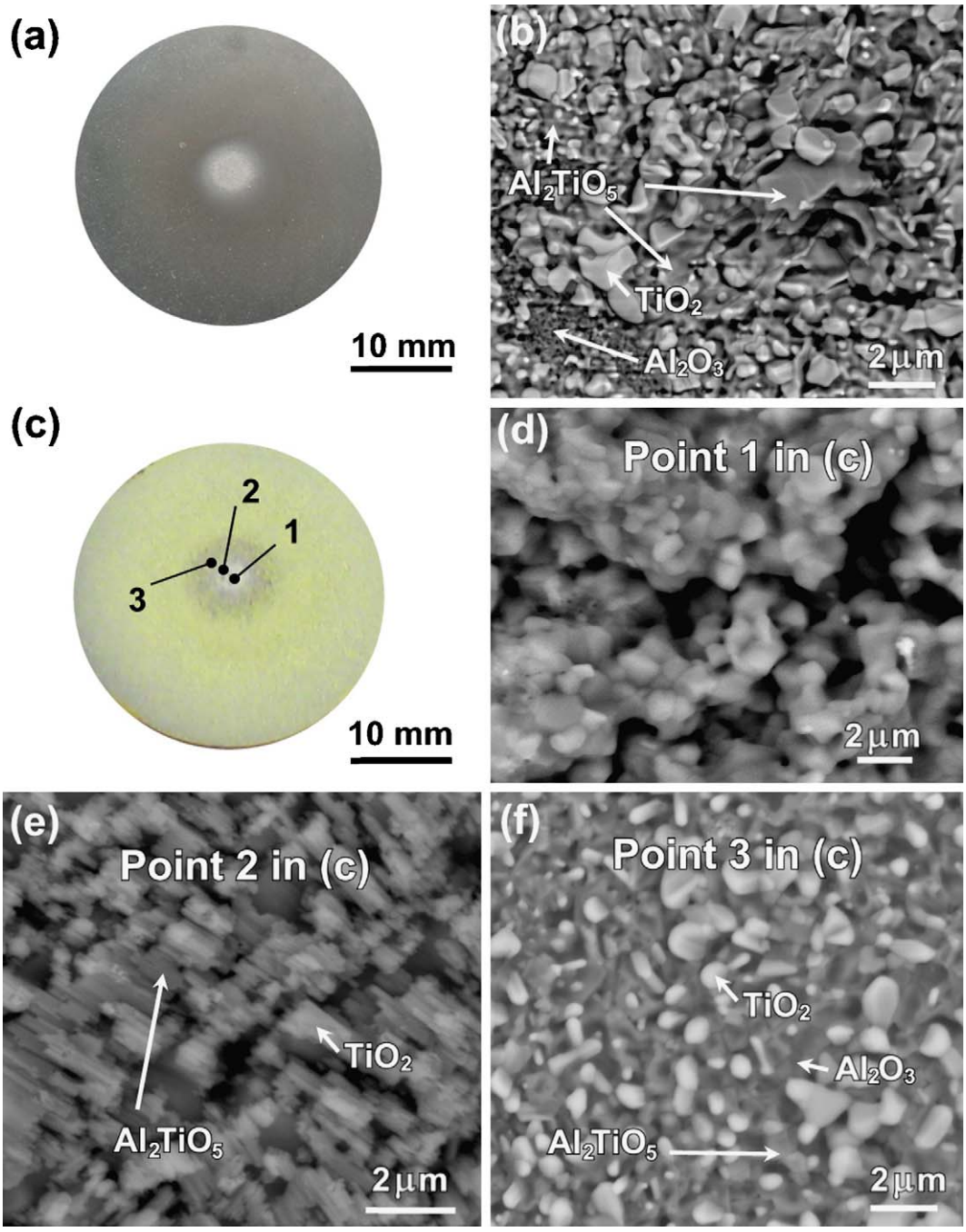

Fig. 4. Surface morphologies of Ti_2AlC after ablation. (a) Macromorphology of the surface after ablation for 30 s; (b) ablation products at the centre zone of the ablated surface in (a); and (c) macromorphology of the surface after ablation for 180 s. High magnification images taken at points of 1, 2 and 3 in (c) show, respectively, the porous ablation layer structure (d), mechanical scour traces (e) and oxidation products (f).

mainly three types of phases, α-Al_2O_3, rutile TiO_2 and Al_2TiO_5, which composed the oxidation layer with voids inside, as indicated with arrows in Fig. 4(b). The particle size of α-Al_2O_3 is about 100–200 nm, which is much smaller than that of the TiO_2 and Al_2TiO_5 particles (roughly about from 0.5 to 1.5 μm). When the ablation time was extended to 180 s, the porous ablation layer at the centre zone (Point 1 in Fig. 4(c)) became looser, as shown in Fig. 4(d). These pores are probably mainly caused by melting and volatilization of the oxides with low melting points (i.e. the melting of TiO_2 (1843 °C) and Al_2TiO_5 (1850 °C)[7] and the evaporation of CO and CO_2). Similar porous structure caused by oxyacetylene flame ablation are often observed in ablative materials where oxidation occurs, like ZrC-doped C/C composites,[18] ZrB_2–SiC doped C/C composites,[19] TiC/W and ZrC/W composites[16,17] and ZrB_2–SiC–ZrO_2 composites.[20] The high magnification image of the area near the centre zone (Point 2 in Fig. 4(c)) reveals a mechanical scour that resulted from the blowing of the firing gas (Fig. 4(e)). Fig. 4(f) is the high magnification image of Point 3 in Fig. 4(c), which shows TiO_2, Al_2TiO_5 particles growing in the α-Al_2O_3 layer.

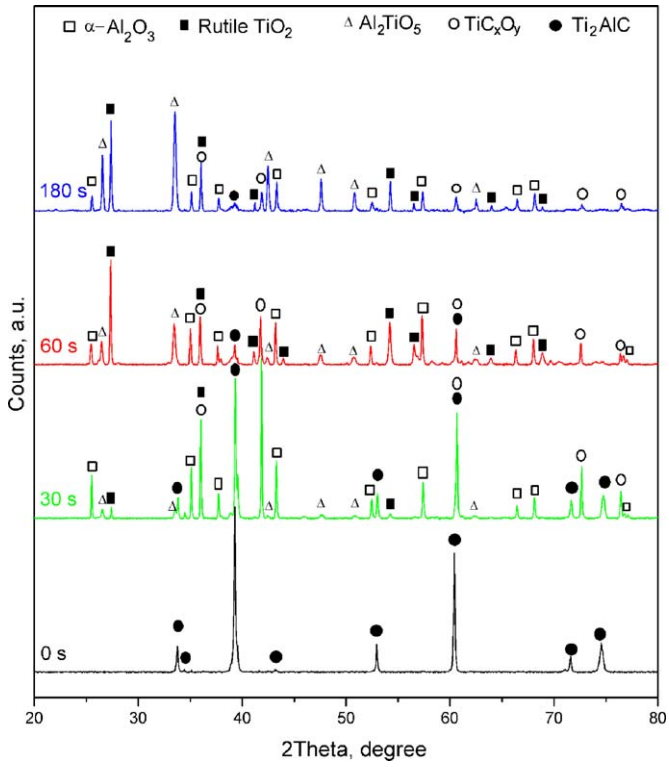

Fig. 5. XRD patterns of the ablated surfaces of Ti_2AlC disks. The identification of phases was according to the ICDD cards No. 04-001-6044 (Ti_2AlC), 01-006-1758 (TiC_xO_y), 04-004-2852 (α-Al_2O_3), 01-073-1782 (rutile TiO_2) and 00-026-0040 (Al_2TiO_5), respectively.

The XRD patterns recorded of the surface centre zone of the original sample and the samples after exposure to the flame for 30, 60 and 180 s are present in Fig. 5. The original material Ti_2AlC contains a small amount of Al_2O_3 particles which was not detected by the XRD due to its low content, as shown in Fig. 1. These patterns show that when the ablation time was shorter than 30 s, the oxidation products are mainly α-Al_2O_3, TiO_2 and minor fractions of Al_2TiO_5. After ablation of longer times, more TiO_2 and Al_2TiO_5 were formed. Furthermore, a titanium oxycarbide (TiC_xO_y, $(x+y) \leq 1$) phase, which can be regarded as a TiC with partial substitution of carbon by oxygen without changing its rock-salt structure,[21] was also detected on the ablated surfaces (see the peaks at 2θ of 41.8 and 72.5° in Fig. 5). The intensity of the peaks corresponding to TiC_xO_y decreased with increasing ablation time, which may imply that this oxycarbide might be less stable than the oxides of TiO_2 and Al_2TiO_5 or even α-Al_2O_3, and/or might stay beneath these oxides.

To understand the microstructure evolution caused by the ultra-high temperature ablation, the cross-section at the surface centre zone of the ablated disk samples was examined with SEM/EDS. The cross sections of the ablated samples are shown in Fig. 6, which reveals that the ablation layer is composed of a thin oxide scale as the outer layer and a thick porous sub-surface layer as the inner layer. With increasing the ablation time from 60 s to 180 s, the thickness of the porous sub-surface layer increased from about 40 μm to 80 μm, together with an increase of the porosity (Fig. 6(a) and (b)). Fig. 6(c) is a high magnification micrograph of the oxide scale in Fig. 6(b) (marked by a yellow box), which clearly shows that the scale mainly consists of Al_2O_3, Al_2TiO_5 and TiO_2 with pores inside (Points A–D in Fig. 6(c) represent Al_2O_3, Al_2TiO_5, TiO_2 phases and pores, respectively). The porous sub-surface layer developing upon ablating is a complex layer containing Ti, Al, C and O, as can be seen from the composition depth profile (Fig. 6(d)) in Fig. 6(b). Composition analysis at Point E in Fig. 6(c) showed 17 at% O, 11 at% C, 54 at% Ti and 18 at% Al, demonstrating that the sub-surface layer is an oxygen rich structure. The average content of the oxygen in this layer is about 22 at%, which is about twice that of the original carbon content.

Ti_2AlC is thermally unstable at temperatures above 1500 °C under vacuum conditions.[22] The decomposition temperature of Ti_2AlC is likely to decrease in an oxidizing environment or/and under pressure.[9,22–25] For example, Ti_2AlC starts to decompose ($Ti_2AlC \rightarrow TiC + TiAl$) at 800 °C under 5 GPa.[22] The shift is due to Al atoms diffusing to the surface of Ti_2AlC bulk to form Al_2O_3, leaving Al vacancies in Ti_2Al_xC matrix as a consequence of the low migration energy of Al for self-diffusion along the (0 0 0 1) plane of Ti_2AlC unit as compared with the those of C and Ti.[23,25] When the Al vacancy concentration exceeds a critical point (50% vacancies on the Al sites according to the ab initio calculations of Wang et al. on Ti_2AlC),[8] a twinned $TiC_{0.5}$ structure might be generated due to the collapse of Ti_2Al_xC structure. When Ti_2AlC is exposed to the oxyacetylene flame with a temperature up to about 3000 °C, the decomposition and oxidation of Ti_2AlC will occur simultaneously. Ti_2AlC can decompose into TiC and TiAl, and meanwhile these products will react with oxygen to form TiC_xO_y oxycarbide, CO or/and CO_2 gases, and Al_2O_3, TiO_2, and Al_2TiO_5 oxides. Moreover, the outward diffusion of Al atoms from the Ti_2AlC matrix under the severe condition of high temperature oxidation will yield the transformation of Ti_2AlC into $TiC_{0.5}$ twins[8] ($TiC_{0.5}$ twins probably intergrew with Ti_2AlC grain) and Al_2O_3. Due to the higher density of TiC_x ($\sim$4.93 g cm^{-3})[7] compared to that of Ti_2AlC (4.11 g cm^{-3}),[4] such a transformation will cause volume shrinkage, and as a result, pores are created unavoidably. Both the Al vacancies and the subsequent pores will enhance the inward diffusion of oxygen into Ti_2Al_xC. With uptake of oxygen, TiC twins are re-constructed as TiC_xO_y. A prior investigation of the selective oxidation of Ti_3AlC_2 powders upon heating in Ar also showed an O-rich porous TiC_xO_y structure developing on Ti_3AlC_2 powders.[26] The research by Sonestedt et al.[27] on the high velocity oxy-fuel sprayed Ti_2AlC coating also showed that Ti_2AlC decomposed into TiC and Ti_xAl_y due to an outward diffusion of Al when Ti_2AlC powers were exposed to a high-energy exhaust flame during the spraying process. Based on the EDS and XRD results, this porous sub-surface layer should be a mixture of $Ti_2Al_{1-x}C$ grains and TiC_xO_y grains (probably intergrowing with each other), which was caused by the decomposition and oxidation of Ti_2AlC. Other phases, like the so-called O-rich Ti_2AlC (or $Ti_2Al_{1-x}C_yO_z$, $(y+z) \leq 1$, which has the same structure as Ti_2AlC, and has been theoretically predicted[28,29] and experimentally confirmed)[29,30] and Ti_xAl_y also may exist in this oxygen rich porous sub-surface layer.

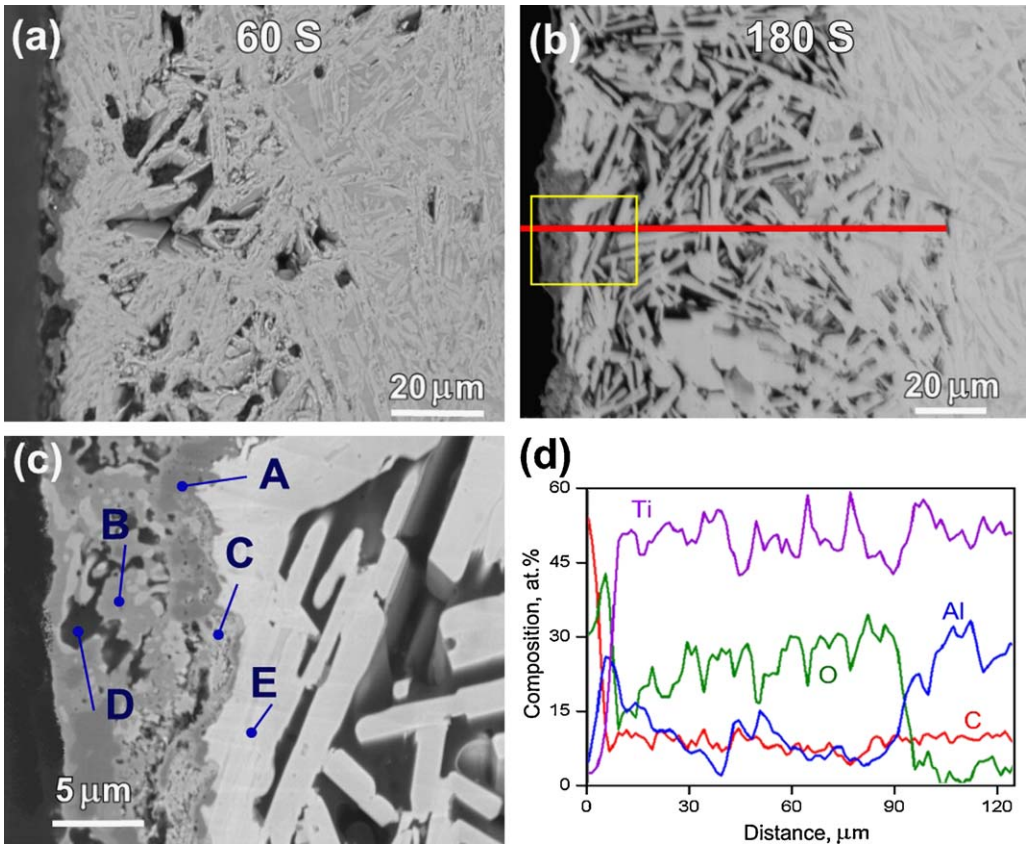

Fig. 6. Cross sections of the ablated Ti_2AlC showing a porous ablation structure developing upon ablation. (a) Cross section of the sample after ablation for 60 s; (b) cross section of the sample after ablation for 180 s; (c) high magnification image of a local area (marked by a yellow box) on the cross section in (b). (A) Al_2O_3, (B) Al_2TiO_5, (C) TiO_2, (D) pores, (E) $TiC_xO_y + Ti_2Al_{1-x}C$; (d) composition depth profile of elements of Ti, Al, C and O of the cross section in (b). (For interpretation of the references to color in this figure legend, the reader is referred to the web version of the article.)

3.3. Ablation mechanisms

During the ablation of the Ti_2AlC under a fast flowing oxy-acetylene flame, a series of complicated physical and chemical processes take place between the ultra-high temperature oxidative gasses and Ti_2AlC. First, Ti_2AlC likely decompose into TiC and TiAl, analogous to the decomposition of Ti_2AlC powders exposed to high velocity oxy-fuel flame[27]:

$$Ti_2AlC \rightarrow TiC + TiAl \quad (3)$$

TiAl (or even Ti_xAl_y) may be an intermediate compound and cannot be detected by XRD, probably due to its low content at the ablated surface. Then these decomposited products may successively react with O_2 to form oxides:

$$TiC + O_2 \rightarrow TiC_xO_y + CO_2\,(\text{or CO}) \quad (4)$$

$$TiC_xO_y + O_2 \rightarrow TiO_2{+}CO_2\,(\text{or CO}) \quad (5)$$

$$TiAl + O_2 \rightarrow TiO_2 + Al_2O_3 \quad (6)$$

Meanwhile, Ti_2AlC also may directly react with O_2:

$$Ti_2AlC + O_2 \rightarrow Ti_2Al_{1-x}C{+}Al_2O_3 + CO_2\,(\text{or CO}), \quad (x < 0.5) \quad (7)$$

$$Ti_2Al_{1-x}C + O_2 \rightarrow TiC_yO_z + Al_2O_3 + CO_2\,(\text{or CO}), \quad ((y+z) \leq 1) \quad (8)$$

$$TiC_xO_y + O_2 \rightarrow TiO_2 + CO_2\,(\text{or CO}) \quad (9)$$

When the temperature is above 1200 °C, TiO_2 and Al_2O_3 will form Al_2TiO_5[5,31]

$$TiO_2 + Al_2O_3 \rightarrow Al_2TiO_5 \quad (10)$$

The oxidation products Al_2O_3, TiO_2 and Al_2TiO_5 comprise the ablation oxide layer. The weight gain upon ablation is attributed to oxidation-induced weight increase, which can be understood via the oxidation Eqs. (4)–(9). With one molar C loss, several molars oxygen is taken up via the formation of solid oxide and oxygen incorporation into the Ti_2AlC matrix to form TiC_xO_y or/and $Ti_2Al_{1-x}C_yO_z((y+z) \leq 1)$. The decomposition of Ti_2AlC at high temperatures may result in the formation of TiC. Meanwhile, the fast outward diffusion of Al from the Ti_2AlC matrix to the sample surface also will create $TiC_{0.5}$ twins. Pores, associated with the volume shrinkage caused by the transformation of Ti_2AlC into $TiC_{0.5}$ twins, will be created too. The pores may also be caused by the emission of CO and CO_2. The Al vacancies in Ti_2AlC lattice and the pores would promote the inward diffusion of oxygen in Ti_2AlC. The

subsequent oxidation of TiC and $TiC_{0.5}$ twins results in formation of TiC_xO_y in $TiAl_2C$ matrix, which should be taken to be responsible for the high oxygen content in the sub-surface layer.

Although the oxyacetylene flame temperature is up to about 3000 °C based on the test condition,[10] the temperature of the ablated surface of a disk will be lower due to heat transfer and dynamic thermal balance existing among the flame, the sample and the environment. Normally, the surface temperature is within the range of 1800–3000 °C depending on the ablated materials and the oxidation products formed on the ablation surfaces, as confirmed by the temperature tests in the prior studies by ourselves[12,16,17] and others.[20,32] The Al_2O_3, TiO_2 and Al_2TiO_5 at the ablated surface will melt, but do not totally evaporate due to their relative high melting points (2053 °C for Al_2O_3, 1843 °C for TiO_2 and 1850 °C for Al_2TiO_5).[7] Due to the existence of an octahedral Ti_2C sub-lattice in the Ti_2AlC lattice, the melting points of Ti_2AlC (or $Ti_2Al_{1-x}C$) and the subsequently formed $TiC_{0.5}$ twins may be very close to that of TiC (~3250 °C),[7] which enables Ti_2AlC to withstand the severe ablation at ultra-high temperatures. The molten TiO_2 and Al_2TiO_5 together with the Al_2O_3 layer is postulated to form a viscous layer limiting the evaporation of CO or/and CO_2, which might result in a volume swelling that in turn leads to the low values of linear ablation rate measured.

The thermal expansion coefficient of Al_2TiO_5 ($\sim 1 \times 10^{-6}\,K^{-1}$)[31] is much lower than that of α-Al_2O_3 ($8.8 \times 10^{-6}\,K^{-1}$ along c axis direction, and $7.9 \times 10^{-6}\,K^{-1}$ normal to c axis direction)[5] and Ti_2AlC ($9 \times 10^{-6}\,K^{-1}$),[5] therefore, the formation of Al_2TiO_5 on the ablated surface may weaken the adhesion of the oxide scale to the Ti_2AlC substrate due to the stress induced by thermal mismatch among these phases,[31] and might finally result in the spallation of the oxide scale when the content of Al_2TiO_5 in the oxide scale is high enough or form a continuous layer. In this study, the Al_2TiO_5 particles existed sporadically at the surface of α-Al_2O_3 layer. Even at the centre zone of the ablated surface, the Al_2TiO_5 did not form a continuous layer due to the relative short ablation time. Therefore, the influence of Al_2TiO_5 on the spallation of the oxide scale could be ignored in this case.

4. Conclusions

The ultra-high temperature ablation properties of Ti_2AlC under a high velocity oxyacetylene flame were examined. The ablated layer formed on the Ti_2AlC surface is of a two-layer structure: a porous oxide outer layer, mainly consisting of α-Al_2O_3 and TiO_2 and Al_2TiO_5, and a porous O-rich sub-surface layer containing $Ti_2Al_{1-x}C$ and TiC_xO_y. With increasing ablation time, the content of TiO_2 and Al_2TiO_5 in the outer layer increased, and more pores developed in the sub-surface layer. After ablation for 180 s, the linear ablation rate and mass ablation rate dropped to low values of 0.08 μm s^{-1} and −180 μg s^{-1}, respectively. The small negative mass rate is caused by the formation of solid oxides. The thermal oxidation of Ti_2AlC and the scouring of the viscous oxidation products by high-speed gas flow are the principal ablation mechanisms.

Acknowledgements

This work was supported by the Delft Center for Materials Research Program on Self Healing Materials and Netherlands Innovation Oriented Program on Self Healing Materials under Grant No. IOP-SHM 0871.

References

1. Barsoum MW. The $M_{n+1}AX_n$ phases: a new class of solids, the thermodynamically stable nanolaminates. *Prog Solid State Chem* 2000;**28**:201–81.
2. Song GM, Pei YT, Sloof WG, Li SB, Van der Zwaag S, De Hosson JThM. Oxidation induced crack healing in Ti_3AlC_2 ceramics. *Scripta Mater* 2008;**58**:13–6.
3. Gauthier-Brunet V, Cabioc'h T, Chartier P, Jaouen M, Dubois S. Reaction synthesis of layered ternary Ti_2AlC ceramic. *J Eur Ceram Soc* 2009;**29**:187–94.
4. Lin ZJ, Zhou MJ, Zhou YC, Li MS, Wang JY. Microstructural characterization of layered ternary Ti_2AlC. *Acta Mater* 2006;**54**:1009–15.
5. Wang XH, Zhou YC. High-temperature oxidation behavior of Ti_2AlC in air. *Oxid Met* 2003;**59**:303–20.
6. Byeon JW, Liu J, Hopkins M, Fischer W, Garimella N, Park KB, et al. Microstructure and residual stress of alumina scale formed on Ti_2AlC at high temperature in air. *Oxid Met* 2007;**68**:97–111.
7. Kosolapova TY, editor. *Handbook of high temperature compounds: properties, production, and application*. New York: Hemisphere Publication; 1990.
8. Wang JY, Zhou YC, Liao T, Zhang J, Lin ZJ. A first-principles investigation of the phase stability of Ti_2AlC with Al vacancies. *Scripta Mater* 2008;**58**:227–30.
9. Liao T, Wang JY, Zhou YC. Ab initio modeling of the formation and migration of monovacancies in Ti_2AlC. *Scripta Mater* 2008;**59**:854–7.
10. National Standard Committee of China. *GJB323A-96: measurement standard of ablation properties of materials*. Beijing; 1996.
11. Gaydon AG, Wolfhard HG, editors. *Flames: their structure, radiation and temperature*. 4th edn. London: Chapman and Hall; 1979.
12. Song GM, Wang YJ, Zhou Y, Lei TC. Measurement of surface temperatrues of a material during ablation. *Min Metall* 2000;**9**:76–80.
13. Erdman N, Campbell R, Asahina S. Artifact-free cross-sections. *Adv Mater Process* 2006;**164**:14–6.
14. Song GM, Pei YT, Sloof WG, Li SB, Van der Zwaag S, De Hosson JThM. Early stages of oxidation of Ti_3AlC_2 ceramics. *Mater Chem Phys* 2008;**112**:762–8.
15. Rusband W. *ImageJ 1.43o software*. USA: National Institute of Health; 2010.
16. Song GM, Wang YJ, Zhou Y. Elevated temperature ablation resistance and thermophysical properties of tungsten matrix composites reinforced with ZrC particles. *J Mater Sci* 2001;**36**:4625–31.
17. Song GM, Wang YJ, Zhou Y. Effect of carbide particles on the ablation properties of tungsten composites. *Mater Charact* 2003;**50**:293–303.
18. Shen XT, Li KZ, Li HJ, Du HY, Cao WF, Lan FT. Microstructure and ablation properties of zirconium carbide doped carbon/carbon composites. *Carbon* 2010;**48**:344–51.
19. Tang SF, Deng JY, Wang SJ, Liu WC, Yang K. Ablation behaviors of ultra-high temperature ceramic composites. *Mater Sci Eng A* 2007;**465**:1–7.
20. Zhou SB, Li WJ, Hu P, Hong CQ, Weng L. Ablation behavior of ZrB_2–SiC–ZrO_2 ceramic composites by means of the oxyacetylene torch. *Corros Sci* 2009;**51**:2071–9.
21. Bellucci A, Gozzi D, Latini A. Overview of the TiC/TiO_2 (rutile) interface. *Solid State Ionics* 2004;**172**:369–75.
22. Qin JQ, He DW, Chen C, Wang JH, Hu J, Yang BW. Phase segregation of titanium–aluminium carbide (Ti_2AlC) at high pressure and high temperature. *J Alloys Compd* 2008;**462**:L24–7.

23. Qin JQ, He DW, Lei L, An P, Fang LM, Li YJ, et al. Differential thermal analysis study of phase segregation of Ti_2AlC under high pressure and high temperature. *J Alloys Compd* 2009;**476**:L8–10.
24. Lin ZJ, Li MS, Wang JY, Zhou YC. Influence of water vapor on the oxidation behavior of Ti_3AlC_2 and Ti_2AlC. *Scripta Mater* 2008;**58**:29–32.
25. Liao T, Wang JY, Li MS, Zhou YC. First-principles study of oxygen incorporation and migration mechanisms in Ti_2AlC. *J Mater Res* 2009;**24**:3190–6.
26. Wang XH, Zhou YC. Stability and selective oxidation of aluminum in nanolaminate Ti_3AlC_2 upon heating in argon. *Chem Mater* 2003;**15**:3716–20.
27. Sonestedt M, Frodelius J, Palmquist JP, Hogberg H, Hultman L, Stiller K. Microstructure of high velocity oxy-fuel sprayed Ti_2AlC coatings. *J Mater Sci* 2010;**45**:2760–9.
28. Dahlqvist M, Alling B, Abrikosov IA, Rosen J. Phase stability of Ti_2AlC upon oxygen incorporation: a first-principles investigation. *Phys Rev B* 2010;**81**:024111.
29. Persson POA, Rosen J, McKenzie DR, Bilek MMM. Formation of the MAX-phase oxycarbide $Ti_2AlC_{1-x}O_x$ studied via electron energy-loss spectroscopy and first-principles calculations. *Phys Rev B* 2009;**80**:092102.
30. Rosen J, Persson POA, Ionescu M, Kondyurin A, McKenzie DR, Bilek MMM. Oxygen incorporation in Ti_2AlC thin films. *Appl Phys Lett* 2008;**92**:064102.
31. Low IM, Oo Z. Reformation of phase composition in decomposed aluminium titanate. *Mater Chem Phys* 2008;**111**:9–12.
32. Han JC, Hu P, Zhang XH, Meng SH, Han WB. Oxidation-resistant ZrB_2–SiC composites at 2200 °C. *Compos Sci Technol* 2008;**68**:799–806.